Journal of Materials Chemistry B

ROYAL SOCIETY OF CHEMISTRY

PAPER

View Article Online
View Journal | View Issue

Published on 27 January 2014. Downloaded by University of Illinois at Chicago on 26/10/2014 15:08:12.

Cite this: J. Mater. Chem. B, 2014, 2, 2013

A highly selective AIE fluorogen for lipid droplet imaging in live cells and green algae†

Erjing Wang,‡[ab] Engui Zhao,‡[ab] Yuning Hong,[ab] Jacky W. Y. Lam[ab] and Ben Zhong Tang*[abc]

Received 27th November 2013
Accepted 27th January 2014

DOI: 10.1039/c3tb21675f

www.rsc.org/MaterialsB

Lipid droplets (LDs) are subcellular organelles for energy storage and lipid metabolism regulation. Here we report an aggregation-induced emission-active fluorogen, TPE-AmAl, for specific LD imaging. TPE-AmAl is cell-permeable: upon entering the live cells, the dye molecules can selectively accumulate in the LDs and turn on the fluorescence. TPE-AmAl possesses twisted intramolecular charge transfer properties as well: the emission colour in the hydrophobic LDs is blue-shifted by >100 nm than that in aqueous buffers. Compared with the commercial lipid droplet dye, TPE-AmAl demonstrates the advantages of low background, short staining time, high selectivity, excellent biocompatibility, and good photostability. The utilization of TPE-AmAl for LD staining in green algae is also demonstrated, indicating their potential application in the high-throughput screening of high-value microalgae as a preferential biofuel source.

Introduction

Lipid droplets (LDs) are the main reservoir for neutral lipid storage and extensively exist in eukaryotic and prokaryotic cells.[1,2] The first discovery of LDs can be traced back to as early as the 17th century[3] and for a long period of time since then, LDs had been simply regarded as a place for energy storage and deemed as an inert cell inclusion.[4] However, the emergence of a series of LD proteins implies that the functions of LDs are more than lipid storage.[5,6] They are dynamic organelles involved in regulating lipid metabolism and storage, membrane transfer, protein degradation, and signal transduction.[7–11] Failure of the regulation may lead to metabolic diseases such as fatty liver disease, atherosclerosis, type II diabetes, and hyperlipidemia.[12] A recent study has revealed another function of LDs as a key organelle for the production and assembly of infectious hepatitis C virus, a causative agent of chronic liver diseases.[13] The abnormality of LDs in cells is a critical biomarker for the related diseases. Moreover, the treatment of certain diseases may also affect the normal level of LDs. For example, LDs appearing in peripheral blood leukocytes are indicative of lipid storage myopathy.[14] The increase of LDs in myofibers is frequently observed during the treatment of inflammatory myopathy,[15] while the decrease of LD volume in adipocytes is indicative of a successful weight loss to some extent.[16]

Monitoring and localizing the accumulation and abnormal level of LDs is thus of particular importance for biomedical research and early diagnosis of the related diseases. In the human body, the liver is the main organ that controls the dynamic balance of lipid metabolism.[17] To assess the LD level and diagnose hyperliposis-related liver diseases, computerized tomography scanning and B-type ultrasound examination are often used. However, these methods are relatively insensitive and only above 25 wt% of the fat content in liver can be detected with reasonable accuracy, which could be diagnosed as the late-stage of severe liver diseases.[18] Diagnosis of early-stage liver diseases including mild fatty liver still relies on transhepatic biopsy to achieve high sensitivity and accuracy.[19] Hence, direct detection of LDs and lipid accumulation in liver tissue still play an important role. In addition to the biomedical significance, the LD is a kind of alternative biofuel for sustainable energy research.[20] Algae are among the best potential sources of biofuel with high efficiency. Therefore, methods for screening algae with high contents of LDs are in high demand.[21]

Fluorescence techniques are powerful tools for studying LDs in living cells and tissues owing to their advantages such as high sensitivity, visibility and tunability in the design of bio-probes.[22] Nile red[23] and BODIPY dyes[24] are widely used for LD imaging. Nile red is a cell-permeable dye that stains most intracellular structures.[25] It emits yellow fluorescence in the nonpolar LDs and red emission in the polar cytosol and other organelles, thus

[a]HKUST-Shenzhen Research Institute, No. 9 Yuexing 1st RD, South Area, Hi-tech Park, Nanshan, Shenzhen, 518057, China. E-mail: tangbenz@ust.hk; Fax: +86-852-2358 1594; Tel: +86-852-2358 7375

[b]Department of Chemistry, Division of Biomedical Engineering, Division of Life Science, State Key laboratory of Molecular Neuroscience, Institute of Molecular Functional Materials and Institute for Advanced Study, The Hong Kong University of Science & Technology, Clear Water Bay, Kowloon, Hong Kong, China

[c]Guangdong Innovative Research Team, SCUT-HKUST Joint Research Laboratory, State Key Laboratory of Luminescent Materials and Device, South China University of Technology, Guangzhou, 510640, China

† Electronic supplementary information (ESI) available: Experimental section, UV-vis and PL emission spectra, and bright field and fluorescent images of living cells. See DOI: 10.1039/c3tb21675f

‡ These authors contributed equally.

Published on 27 January 2014. Downloaded by University of Illinois at Chicago on 26/10/2014 15:08:12.

enabling the discrimination of LDs from others. However, it suffers from low sensitivity because of the high background noise and signal overlap between the two channels. BODIPY dyes, on the other hand, usually have small a Stokes shift.[26] Other stains, such as Oil Red O stain fixed cells only.[27] Besides these drawbacks, traditional fluorophores also encounter the concentration-caused quenching effect.[28] Accumulation of the dye molecules in certain organelles will increase the local dye concentration and result in the self-quenching problem.

To overcome the concentration-quenching problem, a group of fluorogens possessing the aggregation-induced emission (AIE) characteristic are developed.[29] An AIE luminogen is almost non-emissive in the solution state but emits strongly in the aggregate or solid state. Restriction of intramolecular motions has been suggested as the main cause for the AIE phenomenon.[30] Our research group has developed a library of AIE molecules[31] and extensively explored their applications in organic light-emitting diodes, chemo-sensing, bio-probing, *etc.*[32] For bio-imaging, the AIE luminogens exhibit excellent photostability.[33] Hydrophobic AIE luminogens can form nanoaggregates in an aqueous environment. Such nanoaggregates are more resistant to photo-bleaching than a single molecule: even when the molecules on the surface are damaged, they could protect the inner molecules against further photo-bleaching and photo-oxidation. Owing to the superior photostability and biocompatibility, the AIE dyes have been successfully used for specific mitochondria imaging,[33a] full-range intracellular pH mapping,[34] and long-term cell tracking,[35] suggesting them as promising candidates for the new generation of fluorescent dyes for cell research.

From the structural point of view, LD dyes such as Nile red and Seoul-Fluor-based dyes contain both donor (D) and acceptor (A) moieties and experience solvatochroism.[23a,36] Inspired by the structures of these molecules, in this work, we design and synthesize a tetraphenylethene (TPE) derivative (TPE-AmAl) substituted with alkylamino (D) and carbonyl (A) groups. TPE is an archetypical AIE-active luminogen which emits in the blue region. With the D–A moieties, TPE-AmAl emits orange colour in its aggregate state. Systematic studies on the staining of HeLa cells, liver LO2 cells, and green algae are performed, which demonstrate the high selectivity, photostability and biocompatibility of TPE-AmAl for LD imaging.

Results and discussion

Synthesis and optical properties

TPE-AmAl was synthesized according to the synthetic route shown in Scheme 1 in moderate yield. Briefly, McMurry cross-coupling reaction between 4,4′-bis(dimethylamino) benzophenone (**1**) and 4-bromobenzophenone (**2**) generated TPE-AmBr, lithiation and formylation of which gave the designed product TPE-AmAl. The final product was fully characterized by mass and NMR spectroscopies, which confirmed the acquisition of the compounds. TPE-AmAl is completely soluble in common organic solvents such as THF, $CHCl_3$, CH_2Cl_2, DMSO and DMF, but poorly soluble in water.

We then investigated the photophysical properties of TPE-AmAl. From the UV-vis spectrum, the absorption maximum of TPE-AmAl is at ~410 nm in THF solution, which is about 50 nm red-shifted as compared to that of its precursor TPE-AmBr (Fig. S1†). With the absorption maximum in the visible-light region, TPE-AmAl could be used in many biological applications. This red-shift could be ascribed to the presence of the donor–acceptor structures: the dimethylamino group is a strong electron-donating group while the formyl group is an electron-accepting group. The electron push–pull effect narrows the energy gap for electronic transition, corresponding to the bathochromic shift in the absorption spectrum. Increasing the solvent polarity causes a slight red-shift of the absorption maximum (from ~400 to 415 nm) but a large red-shift of the emission maximum (from ~470 to 610 nm), which is a typical phenomenon of twisted intramolecular charge transfer (TICT) (Fig. S2†).

TPE-AmAl is faintly fluorescent in THF and becomes highly emissive in THF–H_2O mixtures with the water fraction larger than 80%, showing a characteristic AIE phenomenon (Fig. 1). Interestingly, with the increase of water fraction from 0 to 70 vol %, the emission maximum is gradually red-shifted (from 525 m to 590 nm) (Fig. 1B). As the polarity of water is much higher than that of THF, increasing the water content leads to a higher polarity of the solvent system and thus red-shifts the emission due to the TICT attribute. Further increase of the water fraction (>70 vol%), however, results in the blue-shift of the emission peak, due to the increasing hydrophobicity of the local environment after the formation of nanoaggregates. The solid-state quantum yield of TPE-AmAl is 22% measured with the integral-sphere technique, which is appreciable for a dye emitting in the orange-to-red region.

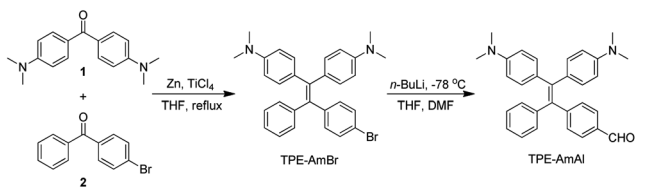

Scheme 1 Synthetic route to TPE-AmAl.

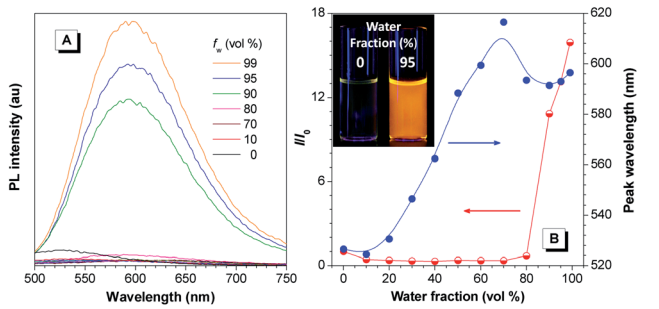

Fig. 1 (A) Emission spectra of TPE-AmAl in THF–water mixtures with different water fractions (f_w). Concentration: 10 μM; excitation wavelength: 410 nm. (B) Plot of the relative PL intensity (I/I_0) and the emission peak wavelength of TPE-AmAl *versus* the water fraction in THF–H_2O mixtures. I_0 = emission intensity in pure THF solution. Inset: photographs of TPE-AmAl (10 μM) in THF–water mixtures with 0 and 95 vol% of water taken under UV illumination.

This journal is © The Royal Society of Chemistry 2014

Published on 27 January 2014. Downloaded by University of Illinois at Chicago on 26/10/2014 15:08:12.

Live cell imaging

Before exploring the application for live cell imaging, we examined the biocompatibility of TPE-AmAl. The cytotoxicity of the dye was evaluated using 3-(4,5-dimethyl-2-thiazolyl)-2,5-diphenyltetrazolium bromide (MTT) assay (Fig. S3†). The results show that no detectable inhibitory effect is observed on the growth of both cervical cancer HeLa cells and liver LO2 cells when up to 100 μM TPE-AmAl is added to the culture media. The excellent biocompatibility of TPE-AmAl motivated us to further investigate their application in cell imaging.

TPE-AmAl was then systematically assessed for its capability to localize in LDs by fluorescence microscopy. HeLa cells were incubated with 10 μM TPE-AmAl for 15 min and the excess dye was washed away with phosphate buffered saline. As shown in Fig. 2A–C, TPE-AmAl enters the live HeLa cells spontaneously and lights up the spherical LDs specifically within a short time (10–15 min is sufficient). The spherical objects in cytosol with distinctly bright fluorescence could be easily identified as LDs. TPE-AmAl is a lipophilic dye which is prone to accumulate in the hydrophobic LDs. Thanks to the AIE property, increasing the concentration of TPE-AmAl in the staining process can enhance the emission intensity in the LDs monotonically without sacrificing the specificity (Fig. S4†).[34,37]

Parallel experiments were performed with Nile red as the stain. Compared with TPE-AmAl which stains the LDs only, Nile red stains not only the LDs (yellow spots) but also other intracellular structures like mitochondria (red emission) (Fig. 2E). The poor specificity makes it difficult to use Nile red as a stain to differentiate LDs from other organelles, not to mention to observe dynamic motions of LDs.

On the other hand, although TPE-AmAl emits an orange color when dispersed in aqueous media, it exhibits a greenish-blue emission in the LD regions (Fig. 1B, inset *vs.* Fig. 2B). This is understandable as the emission of TPE-AmAl is sensitive to the polarity of the environment. The LD is surrounded by a monolayer of phospholipids with the inner part accommodating the hydrophobic tails of the lipids. Therefore, the polarity inside the LDs is much lower. Because of the TICT characteristics, the emission of TPE-AmAl would be at the shorter wavelength region in the LDs environment with low polarity.[38] To verify the hypothesis, the emission spectra of TPE-AmAl in dichloromethane–*n*-hexane mixtures with different polarity were recorded. With an increase of *n*-hexane fraction, the emission peak gradually blue-shifted from 560 to 500 nm (Fig. S5†), showing the polarity-dependent emission of TPE-AmAl.

Oleic acid is known to stimulate cells to produce LDs.[39] Upon treatment with oleic acid for 6 h, the amount of LDs is significantly increased (Fig. 3). The increase of the oleic acid concentration leads to the emergence of more greenish-blue spots in the intracellular region, indicating that more LDs are produced in the cytoplasm. Meanwhile, in the untreated cells, the LDs are located closely to the plasma membrane, while the oleic acid treated cells, the LDs, are trafficked more closely to the nucleus. TPE-AmAl can thus be used to monitor the health of the cells.

Photostability, which is a key parameter for evaluating a fluorescent imaging agent, was examined on TPE-AmAl upon staining the oleic acid-treated HeLa cells. Continuous scanning using a confocal microscope (Zeiss laser scanning confocal microscope LSM7 DUO) was adopted for quantifying the photostability of TPE-AmAl. A dish of oleic acid-treated HeLa cells was incubated with 10 μM TPE-AmAl for 15 min. The initial intensity, which refers to the first scan of HeLa cells stained with TPE-AmAl, was normalized and the remaining fluorescence signals were calculated as a percentage of the initial intensity. As shown in Fig. 4 and S6,† TPE-AmAl selectively enters the LDs in HeLa cells. Even after 55 scans with a total irradiation time span of ~10 min, the signal loss of TPE-AmAl in the cells was less than 20%. No significant difference was

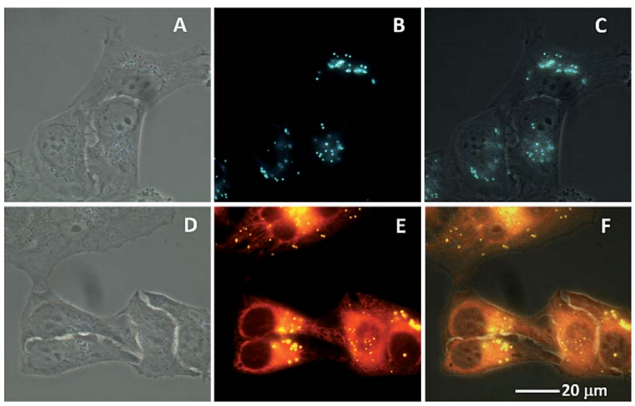

Fig. 2 Images of HeLa cells after incubation with (A–C) TPE-AmAl (10 μM) for 15 min and (D–F) Nile red (100 ng mL^{-1}, 0.314 μM) for 5 min under (A and D) bright field and (B and E) photoexcitation by fluorescence microscopy. (C and F) Merged images of the corresponding bright-field and fluorescence images. Excitation wavelength: 330–385 nm for TPE-AmAl and 460–490 nm for Nile red.

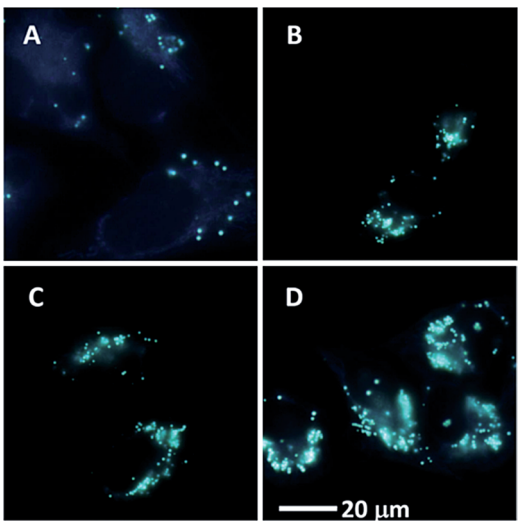

Fig. 3 Fluorescent images of HeLa cells stained with TPE-AmAl (10 μM) for 15 min after incubation in the presence of (A) 0, (B) 12.5, (C) 25 and (D) 50 μM oleic acid for 6 h. Excitation wavelength 330–385 nm.

Published on 27 January 2014. Downloaded by University of Illinois at Chicago on 26/10/2014 15:08:12.

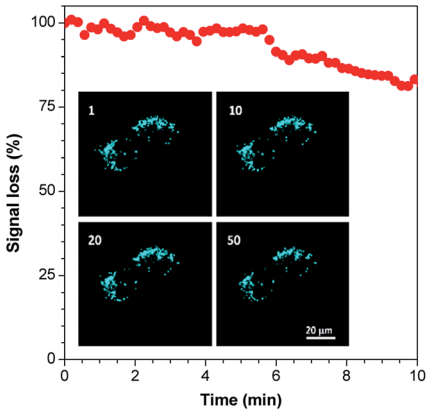

Fig. 4 Signal loss (%) of fluorescence intensity of TPE-AmAl in oleic acid-treated HeLa cells with the scanning time. Inset: fluorescent images of oleic acid-treated HeLa cells stained with TPE-AmAl (10 μM) with increasing numbers of scans (1–55 scans; the number of scans were shown in the upper left corner). Staining time: 15 min; excitation wavelength: 405 nm; emission filter: 449–520 nm; irradiation time: 11.22 s per scan; scale bar: 20 μm.

observed between the first and 50th scans (Fig. 4, inset). The photostability with Nile red (0.314 μM) was also investigated (Fig. S7†). The signal of emission intensity of Nile red in cells decreases about 20% in 2 min irradiation and remains constant thereafter. It is noteworthy that a 0.7% laser power was used for scanning of Nile red experiments while a laser power of 2% was used for TPE-AmAl. In general, the photostability of TPE-AmAl is better than that of Nile red under the same imaging conditions.

The excellent photostability of TPE-AmAl can be attributed to the formation of nanoaggregates and the inert atmosphere inside the hydrophobic LDs. In the culturing medium (MEM) containing 0.1 vol% DMSO – the same condition for HeLa cell imaging – lipophilic TPE-AmAl forms nanoparticles with an average size of ~178 nm, as revealed by particle size analysis (Fig. S8†). The particles can enter the cells and accumulate in the nearly neutral LDs; the hydrophobic and inert environment of LDs could protect the substance against further damage by the external stimuli.

Liver cells are rich in LDs because of the unique function of the liver in lipid metabolism. After treatment of liver LO2 cells with oleic acid, all the cells in a wide view range gave a bluish green emission (Fig. S9†). Similar to the results obtained on HeLa cells, TPE-AmAl could also selectively target the LDs in liver LO2 cells, giving a bluish green emission (Fig. 5A). Compared with HeLa cells, liver LO2 cells produce much more LDs even without the treatment of oleic acid (Fig. S10†).

Exposure of the LO2 cells to increased concentrations of oleic acid can trigger the cells to generate more LDs (Fig. 5). TPE-AmAl can be used to visualize the increase of the LDs, implying its potential application for *in vitro* transhepatic biopsy to assist the diagnosis of early-stage liver diseases. To further verify if all the LDs are stained by TPE-AmAl, Nile red was used for co-staining experiments. As shown in Fig. S11,† all the spherical spots stained by Nile red can be visualized by TPE-AmAl, indicative of the specificity of TPE-AmAl to LDs. Although

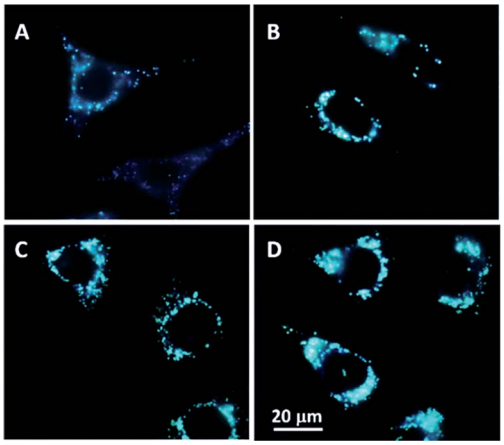

Fig. 5 Fluorescent images of liver LO2 cells stained with TPE-AmAl (10 μM) after incubation in the presence of (A) 0, (B) 12.5, (C) 25 and (D) 50 μM oleic acid for 6 h. Staining time: 15 min; excitation wavelength: 330–385 nm.

Nile red can also image the increase amount of LDs when treated with oleic acid, the background noise from other membrane-bound organelles makes it difficult to be used for LD quantification (Fig. S12†).

Green alga imaging

Algae biofuel research is ascending in the recent decade because of their potential to be an environment-friendly alternative to fossil fuels. The content of lipids is an important parameter to assess the value of the algae. The high selectivity and light up property of TPE-AmAl inspired us to utilize it for the imaging of LDs in algae.

Green algae *Nannochloropsis* sp. was chosen as model algae. To facilitate the diffusion of TPE-AmAl into the algae, different fractions of DMSO containing the same concentration of TPE-AmAl were used in culture media. Higher contents of DMSO result in shorter diffusion times of TPE-AmAl to enter the algal body. When green algae were incubated with 2.5 μM TPE-AmAl at 40 °C for 10 min in the presence of 20% DMSO, a clear image with the lipid content identified by the greenish blue emission of the dye can be acquired (Fig. 6). Note that the red emission colour originates from the chloroplast, which can be differentiated from the LDs under a fluorescence microscope. The

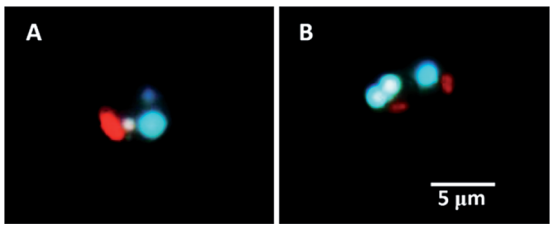

Fig. 6 Fluorescent images of green algae stained with TPE-AmAl (2.5 μM) in the presence of (A) 10 vol% and (B) 20 vol% DMSO at 40 °C for 10 min. Excitation wavelength: 330–385 nm. The blue emission is from the LDs; the red emission is from the chloroplast.

This journal is © The Royal Society of Chemistry 2014

Published on 27 January 2014. Downloaded by University of Illinois at Chicago on 26/10/2014 15:08:12.

diameter of green emission region reflects the size of LDs, while the overall brightness of the image could be correlated with the total lipid content in the LD body. These results demonstrate the feasibility of using TPE-AmAl for high-throughput screening of algae species with high bio-fuel contents.

Conclusion

In summary, an AIE-active TPE derivative, TPE-AmAl, is synthesized and utilized as a fluorescent agent for LD imaging in live HeLa cells, liver LO2 cells and green algae. With the advantages of high selectivity, excellent biocompatibility, high photostability, and simplicity, TPE-AmAl represents an excellent probe for selective imaging and tracking of LDs. The reason for the high affinity to LDs is proposed to be the hydrophobic interaction between TPE-AmAl and LDs. Once entering LDs, the intramolecular motion of TPE-AmAl will be restricted and the emission from TPE-AmAl will be turned on; because of the low polarity inside LDs, TPE-AmAl emits a greenish blue colour distinct from the extracellular orange emission. Collectively, TPE-AmAl exhibits a much lower background noise and higher sensitivity when compared with commercial LD dyes. TPE-AmAl could find a wide range of applications such as in auxiliary diagnosis of early-stage fatty liver disease, monitoring of macrophage foam cells, screening of high-throughput algae for biofuels, searching for oil-producing bacteria, and other aspects.

Materials and methods

General

Tetrahydrofuran (THF) was distilled from a sodium–benzophenone system in a nitrogen atmosphere under normal pressure immediately prior to use. DMF was purified using an ion-exchanged resin purification system. Other solvents were directly used without further purification. The reagents, 4,4′-bis(dimethylamino)benzophenone, 4-bromobenzophenone, zinc, titanium(IV) chloride, *n*-butyl lithium (2.0 M in cyclohexane), oleic acid, Nile red, and ammonium chloride were purchased from commercial companies and directly used without purification. For the biological study, minimum essential medium (MEM), fetal bovine serum (FBS), and RPM 1640 medium were purchased from Invitrogen. The green algae in culture medium was a present from Prof. Ka Ming Ng's group in HKUST.

Instrumentation

^{1}H and ^{13}C-NMR spectra were recorded on a Bruker ARX 400 spectrometer using $CDCl_3$ as the solvent and tetramethyl silane (TMS) as the internal standard. High-resolution mass spectra (HRMS) were recorded on a GCT premier CAB048 mass spectrometer operated in a MALDI-TOF mode. UV-vis absorption spectra were recorded on a Milton Roy Spectronic 3000 Array spectrometer. Photoluminescence spectra were recorded on a Perkin-Elmer LS 55 spectrofluorometer. The $\Phi_{F,f}$ value of solid powder was determined using an integrating sphere method. Particle size analysis was determined at room temperature using a ZetaPlus Potential Analyzer (Brookhaven Instruments Corporation, USA).

Synthesis

Preparation of TPE-AmBr.[40] To an oven-dried two-necked flask 4,4′-bis(dimethylamino)benzophenone (**1**) (3 g, 11.2 mmol), 4-bromobenzophenone (**2**) (3.78 g, 14.5 mmol) and zinc dust (4.18 g, 64 mmol) were added. The mixture was degassed while purging nitrogen at least three times, and then freshly distilled fresh THF (80 mL) was injected into the flask. The reaction system was cooled to −78 °C in a dry ice-acetone bath for at least 15 min. $TiCl_4$ (6.11 g, 32.3 mmol) was added dropwise, after which the reaction was continued for about 8 h under refluxing. The excess zinc was filtered after cooling to room temperature. Aqueous potassium carbonate was added, the mixture was extracted with dichloromethane, and the filtrate was dried with anhydrous magnesium sulfate. After removing the solvent with a rotary evaporator, and the residue was purified with a silica gel chromatographic column using petroleum ether/ethyl acetate (5 : 1) as the eluent to afford a yellow solid as the product 2.33 g. Yield 42%. HR-MS (MALDI-TOF): calcd for $C_{30}H_{29}BrN_2$ 496.1514, found: 496.1523. ^{1}H-NMR (400 MHz, $CDCl_3$) δ 7.23–7.17 (m, 2H), 7.14–7.05 (m, 3H), 7.05–6.99 (m, 2H), 6.94–6.91 (m, 1H), 6.91–6.83 (m, 5H), 6.51–6.40 (m, 4H), 2.90 (d, $J = 11.0$ Hz, 12H). ^{13}C-NMR (100 MHz, $CDCl_3$) δ 148.14, 148.08, 144.01, 143.54, 141.16, 134.63, 132.45, 131.88, 131.85, 131.74, 131.71, 131.11, 131.01, 130.73, 129.90, 126.90, 126.75, 124.92, 118.50, 110.73, 110.62, 110.53, 110.46, 39.56.

Preparation of TPE-AmAl.[41] TPE-AmBr (1.5 g, 0.3 mmol) was added to a 100 mL two-necked flask with nitrogen purging. Dry THF (40 mL) was injected into the reactor and the mixture was cooled to −78 °C in a dry ice-acetone bath for at least 15 min. Then 1.8 mL *n*-BuLi (2 M in cyclohexane) was slowly added dropwise and the temperature was kept at −78 °C for 2 h. Dried DMF (2 mL) was added and the mixture was slowly recovered to room temperature and continued stirring for 2 h. After using saturated ammonium chloride to quench the reaction, the mixture was extracted with dichloromethane and dried with magnesium sulfate. The organic solvent was removed through rotary evaporation under reduced pressure. The residue was purified on a silica column using petroleum ether and dichloromethane for gradient eluting to afford an orange yellow solid product 0.85 g. Yield 63%. HR-MS (MALDI-TOF) calcd for $C_{31}H_{30}N_2O$ 446.2358, found 446.2350. ^{1}H-NMR (400 MHz, $CDCl_3$) δ 9.88 (s, 1H), 7.60 (d, $J = 6.8$ Hz, 2H), 7.18 (d, $J = 7.6$ Hz, 2H), 7.13–7.08 (m, 3H), 7.04–7.02 (m, 2H), 6.91–6.87 (m, 4H), 6.44 (d, $J = 8.8$ Hz, 4H), 2.90 (s, 12H). ^{13}C-NMR (100 MHz, $CDCl_3$) δ 192.27, 152.81, 149.48, 149.33, 144.80, 144.04, 135.68, 133.65, 132.96, 132.86, 132.72, 132.37, 131.82, 131.67, 131.60, 129.36, 128.08, 126.16, 111.75, 111.40, 40.50.

Cell viability evaluated by MTT assay

Cells were seeded in 96-well plates at a density of 5000 cells per well. After overnight culturing, medium in each wells were replaced by fresh medium containing different concentrations

Published on 27 January 2014. Downloaded by University of Illinois at Chicago on 26/10/2014 15:08:12.

of TPE-AmAl. After 24 hours of treatment, into each well, 10 μL MTT solution (5 mg mL^{-1} in phosphate buffer solution) was added. After 4 hours of incubation at 37 °C, 100 μL SDS–HCl solution (10% SDS and 0.01 M HCl) was added to each well. After incubation at 37 °C for 6 hours, the absorbance of each well at 595 nm was recorded using a plate reader (Perkin-Elmer Victor3™). Each of the experiments was performed at least 5 times as a parallel test.

Cell culture and imaging

Cell culture. HeLa cells were cultured in MEM containing 10% FBS and antibiotics (100 units per mL penicillin and 100 μg mL^{-1} streptomycin) in a 5% CO_2 humidity incubator at 37 °C, and liver LO2 cells were cultured in the RPM 1640 medium in a 5% CO_2 humidity incubator at 37 °C.

Cell imaging. HeLa cells were grown overnight on a 35 mm Petri dish with a cover slip or a plasma-treated 25 mm round cover slip mounted on the bottom of a 35 mm Petri dish with an observation window. The liver cells were stained with 10 μM TPE-AmAl for 15 min, 30 min, 45 min, 1 h, or 2 h (by adding 2 μL of a 10^{-3} M stock solution of TPE-AmAl in DMSO to a 2 mL culture medium) or 0.314 μM of Nile red for 5 min (by adding 2 μL of a 0.314 mM stock solution of Nile red in DMSO to a 2 mL culture medium). The cells were imaged under an FL microscope (BX41 Microscope) using proper excitation and emission filters for each dye: for TPE-AmAl, excitation filter = 330–385 nm, dichroic mirror = 400 nm, and emission filter = 420 nm long pass; for Nile red, excitation filter = 460–490 nm, dichroic mirror = 600 nm, and emission filter = 610 nm long pass.

For the photostability test, the cells were imaged using a confocal microscope (Zeiss Laser Scanning Confocal Microscope; LSM7 DUO) using ZEN 2009 software (Carl Zeiss). TPE-AmAl was excited at 405 nm (2% laser power) and the fluorescence was collected at 449–520 nm. Nile red was excited at 488 nm (0.7% laser power) and the fluorescence was collected at 489–633 nm. The scanning speed is 11.22 s per scan.

Cell treatment with oleic acid. HeLa cells (or liver LO2 cells) were grown overnight on a 35 mm Petri dish with a cover slip. The cells were incubated with different concentrations of oleic acid (12.5, 25, and 50 μM) (by adding an appropriate volume of a 50 mM stock solution of oleic acid in DMSO to a 2 mL culture medium) for 6 h. The oleic acid-treated cells were then stained with 10 μM TPE-AmAl for 15 min.

Green algae treatment for imaging. Green algae *Nannochloropsis* sp. in culture medium were donated by Prof. Ka Ming Ng's group in HKUST. For algae imaging, different fractions of DMSO containing TPE-AmAl were added to the medium, after which the medium containing the algae was placed in a water bath at 40 °C for 10 min. Then the sample was directly transferred to a platform for cell imaging under a fluorescence microscope.

Acknowledgements

This work was partially supported by the National Basic Research Program of China (973 Program; 2013CB834701), the Research Grants Council of Hong Kong (604711, 604913, HKUST2/CRF/10 and N_HKUST620/11), and the University Grants Committee of Hong Kong (AoE/P-03/08). B.Z.T. thanks the Guangdong Innovative Research Team Program for support (201101C0105067115).

Notes and references

1 D. J. Murphy, *Prog. Lipid Res.*, 2001, **40**, 325–438.
2 J. K. Zehmer, Y. Huang, G. Peng, J. Pu, R. G. Anderson and P. Liu, *Proteomics*, 2009, **9**, 914–921.
3 E. A. Kernohan and E. E. Lepherd, *J. Dairy Res.*, 1969, **36**, 177–182.
4 S. Martin and R. G. Parton, *Nat. Rev. Mol. Cell Biol.*, 2006, **7**, 373–378.
5 H.-P. Jiang and G. Serrero, *Proc. Natl. Acad. Sci. U. S. A.*, 1992, **89**, 7856–7860.
6 N. E. Wolins, B. Rubin and D. L. Brasaemle, *J. Biol. Chem.*, 2001, **276**, 5101–5108.
7 H. Zhang, Y. Wang, J. Li, J. Yu, J. Pu, L. Li, H. Zhang, S. Zhang, G. Peng, F. Yang and P. Liu, *J. Proteome Res.*, 2011, **10**, 4757–4768.
8 K. Atheenstaedt, D. Zweytick, A. Jandrositz, S. D. Kohlwein and G. Daum, *J. Bacteriol.*, 1999, **181**, 6441–6448.
9 E. J. Blanchette-Mackie, N. K. Dwyer, T. Barber, R. A. Coxey, T. Takeda, C. M. Rondinone, J. L. Theodorakis, A. S. Greenberg and C. Londos, *J. Lipid Res.*, 1995, **36**, 1211–1226.
10 A. W. Cohen, B. Razani, W. Schubert, T. M. Williams, X. B. Wang, P. Lyengar, D. L. Brasaemle, P. E. Scherer and M. P. Lisanti, *Diabetes*, 2004, **53**, 1261–1270.
11 R. A. Bascom, H. Chan and R. A. Tachubinski, *Mol. Biol. Cell*, 2003, **14**, 939–957.
12 K. G. M. M. Alberti, P. Zimmet and J. Shaw, *Lancet*, 2005, **366**, 1059–1062.
13 (*a*) S. Boulant, P. Targett-Adams and J. McLauchlan, *J. Gen. Virol.*, 2007, **88**, 2204–2213; (*b*) Y. Miyanari, K. Atsuzawa, N. Usuda, K. Watashi, T. Hishiki, M. Zayas, R. Bartenschlager, T. Wakita, M. Hijikata and K. Shimotohno, *Nat. Cell Biol.*, 2007, **9**, 1089–1097.
14 W.-C. Liang and I. Nishino, *Curr. Neurol. Neurosci. Rep.*, 2011, **11**, 97–103.
15 E. E. Calore, A. Sesso, F. R. Puga, M. J. Cavaliere, N. M. P. Calore and R. Weg, *Exp. Toxicol. Pathol.*, 1999, **51**, 27–33.
16 I. Vermaak, A. M. Viljoen and J. H. Hamman, *Nat. Prod. Rep.*, 2011, **28**, 1493–1533.
17 J. Davis, A. E. Crunk, J. Monks, A. Murakami, M. Jackman, P. S. MacLean, M. Ladinsky, E. S. Bales, S. Cain, D. J. Orlicky and J. L. McManaman, *PLoS One*, 2013, **8**, e67631.
18 T. Yonezawa, R. Kurata, M. Kimura and H. Inoko, *Mol. BioSyst.*, 2011, **7**(1), 91–100.
19 (*a*) R. W. Chapman, *Gut*, 2002, **51**, 9–10; (*b*) M. M. Skelly, P. D. James and S. D. Ryder, *J. Hepatol.*, 2001, **35**, 195–199.
20 R. H. Wijffels and M. J. Barbosa, *Science*, 2010, **329**, 796–799.

 This journal is © The Royal Society of Chemistry 2014

Published on 27 January 2014. Downloaded by University of Illinois at Chicago on 26/10/2014 15:08:12.

21 Y. Ding, S. Zhang, L. Yang, H. Na, P. Zhang, H. Zhang, Y. Wang, Y. Chen, J. Yu, C. Huo, S. Xu, M. Garaiova, Y. Cong and P. Liu, *Nat. Protoc.*, 2012, **8**, 43–51.
22 S. M. Borisov and O. S. Wolfbeis, *Chem. Rev.*, 2008, **108**, 423–461.
23 (*a*) P. Greenspan, E. P. Mayer and S. D. Fowler, *J. Cell Biol.*, 1985, **100**, 965–973; (*b*) K. S. Jones, A. P. Alimov, H. L. Rilo, R. J. Jandacek, L. A. Woollett and W. T. Penberthy, *Nutr. Metab.*, 2008, **5**, 23–33.
24 (*a*) J. Spandl, D. J. White, J. Peychl and C. Thiele, *Traffic*, 2009, **10**, 1579–1584; (*b*) Y. Ohsaki, Y. Shinohara, M. Suzuki and T. Fujimoto, *Histochem. Cell Biol.*, 2010, **133**, 477–480.
25 P. M. Gocze and D. A. Freeman, *Cytometry*, 1994, **17**, 151–158.
26 A. Loudet and K. Burgess, *Chem. Rev.*, 2007, **107**, 4891–4932.
27 (*a*) E. J. O'Rourke, A. A. Soukas, C. E. Carr and G. Ruvkun, *Cell Metab.*, 2009, **10**, 430–435; (*b*) K. Yen, T. T. Le, A. Bansal, S. D. Narasimhan, J.-X. Cheng and H. A. Tissenbaum, *PLoS One*, 2010, **5**, e12810.
28 T. Förster and K. Kasper, *Z. Phys. Chem.*, 1954, **1**, 275–277.
29 J. Luo, Z. Xie, J. W. Y. Lam, L. Cheng, H. Chen, C. Qiu, H. S. Kwok, X. Zhan, Y. Liu, D. Zhu and B. Z. Tang, *Chem. Commun.*, 2001, 1740–1741.
30 (*a*) Y. Dong, J. W. Y. Lam, A. Qin, J. Sun, J. Liu, Z. Li, J. Sun, H. H. Y. Sung, I. D. Williams, H. S. Kwok and B. Z. Tang, *Chem. Commun.*, 2007, 3255–3257; (*b*) Z. Li, Y. Dong, B. Mi, Y. Tang, M. Häussler, H. Tong, Y. Dong, J. W. Y. Lam, Y. Ren, H. H. Y. Sung, K. S. Wong, P. Gao, I. D. Williams, H. S. Kwok and B. Z. Tang, *J. Phys. Chem. B*, 2005, **109**, 10061–10066; (*c*) Q. Zeng, Z. Li, Y. Dong, C. Di, A. Qin, Y. Hong, L. Ji, Z. Zhu, C. K. W. Jim, G. Yu, Q. Li, Z. Li, Y. Liu, J. Qin and B. Z. Tang, *Chem. Commun.*, 2007, 70–72.
31 (*a*) Y. Hong, J. W. Y. Lam and B. Z. Tang, *Chem. Commun.*, 2009, 4332–4353; (*b*) J. Liu, J. W. Y. Lam and B. Z. Tang, *Chem. Rev.*, 2009, **109**, 5799–5867; (*c*) Y. Hong, J. W. Y. Lam and B. Z. Tang, *Chem. Soc. Rev.*, 2011, **40**, 5361–5388.
32 Z. Zhao, J. W. Y. Lam and B. Z. Tang, *J. Mater. Chem.*, 2012, **22**, 23726–23740.
33 (*a*) C. W. T. Leung, Y. Hong, S. Chen, E. Zhao, J. W. Y. Lam and B. Z. Tang, *J. Am. Chem. Soc.*, 2013, **135**, 62–65; (*b*) N. Zhao, M. Li, Y. Yan, J. W. Y. Lam, Y. L. Zhang, Y. S. Zhao, K. S. Wong and B. Z. Tang, *J. Mater. Chem. C*, 2013, **1**, 4640–4646.
34 S. Chen, Y. Hong, Y. Liu, J. Liu, C. W. T. Leung, M. Li, R. T. K. Kwok, E. Zhao, J. W. Y. Lam, Y. Yu and B. Z. Tang, *J. Am. Chem. Soc.*, 2013, **135**, 4926–4929.
35 Z. Wang, S. Chen, J. W. Y. Lam, W. Qin, R. T. K. Kwok, N. Xie, Q. Hu and B. Z. Tang, *J. Am. Chem. Soc.*, 2012, **135**, 8238–8245.
36 (*a*) E. Kim, S. Lee and S. B. Park, *Chem. Commun.*, 2012, **48**, 2331–2333; (*b*) Y. Lee, S. Na, S. Lee, N. L. Jeon and S. B. Park, *Mol. BioSyst.*, 2013, **9**, 952–956; (*c*) S. Lee, E. Kim and S. B. Park, *Chem. Sci.*, 2013, **4**, 3282–3287.
37 (*a*) Y. Hong, L. Meng, S. Chen, C. W. T. Leung, L.-T. Da, M. Faisal, D.-A. Silva, J. Liu, J. W. Y. Lam, X. Huang and B. Z. Tang, *J. Am. Chem. Soc.*, 2012, **134**, 1680–1689; (*b*) S. Chen, J. Liu, Y. Liu, H. Su, Y. Hong, C. K. W. Jim, R. T. K. Kwok, N. Zhao, W. Qin, J. W. Y. Lam, K. S. Wong and B. Z. Tang, *Chem. Sci.*, 2012, **3**, 1804–1809.
38 (*a*) W. Rettlg, *J. Phys. Chem.*, 1982, **86**, 1970–1976; (*b*) M. Koenig, G. Bottari, G. Brancato, V. Barone, D. M. Guldi and T. Torres, *Chem. Sci.*, 2013, **4**, 2502–2511; (*c*) Z. R. Grabowski and K. Rotkiewicz, *Chem. Rev.*, 2003, **103**, 3899–4032.
39 Y. Fujimoto, J. Onoduka, K. J. Homma, S. Yamaguchi, M. Mori, Y. Higashi, M. Makita, T. Kinoshita, J.-i. Noda, H. Itabe and T. Takano, *Biol. Pharm. Bull.*, 2006, **29**, 2174–2180.
40 Q. Zhao, K. Li, S. Chen, A. Qin, D. Ding, S. Zhang, Y. Liu, B. Liu, J. Z. Sun and B. Z. Tang, *J. Mater. Chem.*, 2012, **22**, 15128–15135.
41 R. Hu, J. L. Maldonado, M. Rodriguez, C. Deng, C. K. W. Jim, J. W. Y. Lam, M. M. F. Yuen, G. Ramos-Ortiz and B. Z. Tang, *J. Mater. Chem.*, 2012, **22**, 232–240.